

Latent-Space Autoregressive World Model for Efficient and Robust Image-Goal Navigation

Zhiwei Zhang Hui Zhang Xieyuanli Chen Kaihong Huang Chenghao Shi* Huimin Lu

Abstract—Traditional navigation methods rely heavily on accurate localization and mapping. In contrast, world models that capture environmental dynamics in latent space have opened up new perspectives for navigation tasks, enabling systems to move beyond traditional multi-module pipelines. However, world model often suffers from high computational costs in both training and inference. To address this, we propose LS-NWM—a lightweight latent space navigation world model that is trained and operates entirely in latent space, compared to the state-of-the-art baseline, our method reduces training time by approximately 3.2 \times and planning time by about 447 \times , while further improving navigation performance with a 35% higher SR and an 11% higher SPL. The key idea is that accurate pixel-wise environmental prediction is unnecessary for navigation. Instead, the model predicts future latent states based on current observational features and action inputs, then performs path planning and decision-making within this compact representation, significantly improving computational efficiency. By incorporating an autoregressive multi-frame prediction strategy during training, the model effectively captures long-term spatiotemporal dependencies, thereby enhancing navigation performance in complex scenarios. Experimental results demonstrate that our method achieves state-of-the-art navigation performance while maintaining a substantial efficiency advantage over existing approaches.

I. INTRODUCTION

Autonomous navigation is a critical topic in robotics and has evolved over many years into a framework comprising several established components, that is, localization, mapping, planning, and control [1], [2], [3]. However, such complex modular designs often lead to high maintenance costs and accumulated errors. To address this issue, substantial efforts have been made in imitation learning [4], [5], [6] and reinforcement learning [7], [8] to achieve end-to-end navigation. However, reinforcement learning faces issues of sample efficiency and security risks, while imitation learning relies on expert data and has limited generalization ability. Inspired by the human ability to imagine the spatial layout of surroundings and plan trajectories during navigation, world model-based methodologies [9] have recently attracted considerable attention. By simulating potential environmental changes in “mind”—like humans—world models allow agents to conduct counterfactual reasoning over potential future states, thereby facilitating end-to-end navigation.

All the authors are with the College of Intelligence Science and Technology, and the National Key Laboratory of Equipment State Sensing and Smart Support, National University of Defense Technology, China.

This work has partially been funded by the Youth Independent Innovation Science Fund Project of the National University of Defense Technology (Grant ZK25-50), by the National Science Foundation of China (Grant No. 62403478), by Young Elite Scientists Sponsorship Program by CAST (No. 2023QNRC001)

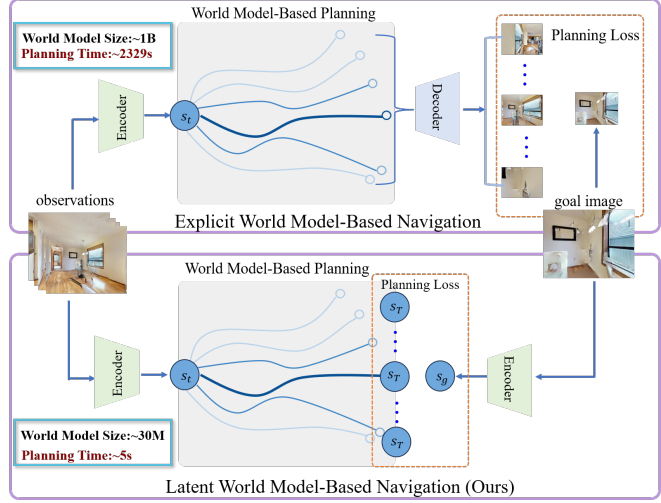


Fig. 1: Common world model-based planning approaches typically represent and plan future states in explicit pixel space. Pixel-level reconstruction and planning results in large model size and high computational demands. In contrast, our method conducts both prediction and planning in latent space, significantly reducing computational load and model size while maintaining comparable or even superior performance.

However, how to construct such a navigation world model remains an open research question.

World models can generally be divided into two categories [10]: those that learn implicit representations and those that predict future states. Implicit representation methods convert external realities into structured latent tokens to support traditional decision-making pipelines. However, such methods are currently limited to predicting specific objects and fail to capture the holistic dynamics of the entire environment. On the other hand, future state prediction approaches model environmental evolution by generating discrete or static future states. With progress in video-like simulation capable of modeling continuous spatiotemporal changes, recent world models [9], [11], [12] have been designed to operate in more complex and dynamic settings. Yet, achieving high-quality video generation requires substantial computational resources, as in methods like NWM [9], typically requires substantial computational resources, making these methods difficult to deploy on real robotic platforms. This raises an important question: is high-quality video generation actually necessary for navigation? Much like humans who selectively focus on a sparse set of salient elements rather than reconstructing every detail, we hold that navigation does not require pixel-perfect future frames. To this end, we propose

LS-NWM, a lightweight navigation world model that operates in latent space, leveraging sparse implicit scene features to predict future states and enable end-to-end navigation.

The main contributions of this work are summarized as follows. We propose LS-NWM, a lightweight latent space navigation world model that supports end-to-end image-goal navigation by predicting future latent states instead of pixel-level video sequences, drastically reducing memory and computational requirements. Our design enables efficient planning and decision-making directly in latent space. We introduce an autoregressive multi-frame prediction strategy to capture long-term spatiotemporal dependencies, enhancing the model's ability to forecast future states and plan trajectories in complex navigation scenarios. Extensive experiments are conducted to demonstrate the effectiveness of our method in trajectory prediction for the image-goal navigation task. Furthermore, we validate in simulation environments that our approach achieves state-of-the-art image-goal navigation performance compared to baseline methods.

II. RELATED WORK

Visual Navigation Visual navigation is essential for autonomous robots, enabling them to perceive their environment and generate appropriate paths towards a target. In traditional visual navigation, a robot's navigation capability relies heavily on accurate visual perception and effective path planning algorithms [13], [14]. Recent research has incorporated deep learning and reinforcement learning [15], [8], [7] techniques into visual navigation to enhance the robot's adaptability in environments. For instance, the NoMaD model [6] uses a unified diffusion strategy for both target image navigation and exploration tasks, while NavDP [16] combines diffusion-based trajectory generation with an evaluation function for efficient real-world navigation. PoliFormer [8] employs large-scale reinforcement learning for end-to-end training, improving practicality and adaptability. Additionally, Vision-language models (VLMs) can organically integrate natural language instructions with visual inputs [17], [18], [19], [20]. They not only facilitate target localization but also infer the relationships between targets and surrounding objects, thereby providing guidance for navigation. Despite recent progress, existing methods face challenges in generalizing to dynamic environments and high-dimensional perceptual tasks, where high computational costs and limited inference efficiency remain critical bottlenecks.

World Model for Navigation Recently, world models have emerged as a powerful framework, achieving significant advances in both simulated environments [21] and reinforcement learning [22], [23], [24]. In the field of world model research, such models generally serve two core functions: first, constructing internal representations to interpret the world, and second, predicting future states to simulate and guide decision-making. From the perspective of environmental understanding, autonomous navigation requires building accurate perceptual and internal representations of the external world to discern object structures, states, and

their interrelationships—a fundamental prerequisite for effective navigation. Focusing on data-driven implicit memory, world models learn semantic, geometric, and physical regularities present in the environment, thereby forming flexible and adaptive world representations. WMNav [25] integrates Vision-language models (VLMs) into the world model framework for goal navigation tasks. By leveraging panoramic image prompts, the VLM estimates the likelihood of target presence in different directions and generates a Curiosity Value Map, which quantitatively stores semantic information about the environment. Pathdreamer [12] reprojects point clouds into 2D guiding images, from which it generates high-resolution RGB images, semantic segmentation maps, and depth maps to support the robot's understanding of the spatial layout in unknown regions. DreamWalker [11], on the other hand, constructs discrete, structured abstractions of continuous environments and conducts extensive simulations to enable efficient, strategy-oriented planning. From the perspective of future prediction, autonomous navigation requires anticipating environmental changes and the consequences of actions to preemptively plan feasible paths and adapt to complex, dynamic scenarios. World models learn environmental dynamics to predict future states under various action sequences, thereby supporting globally optimized decision-making for robotic systems. The Navigation World Model (NWM) [9], built upon a Conditional Diffusion Transformer (CDiT) architecture, is trained on large-scale robot and agent video datasets. It predicts future visual observations conditioned on the current world state and navigation actions. X-Mobility [26] simulates diverse terrains, such as grass, sand, and concrete in virtual environments to model their influence on robot motion and predict corresponding movement outcomes.

Although visual navigation and world models have demonstrated considerable potential in simulated and experimental settings, vision-based navigation methods remain heavily dependent on the robot's perceptual capabilities [27], [28], which are constrained by image quality and perception accuracy. Furthermore, many generative world models, such as diffusion-based approaches, though capable of producing diverse trajectories and predicting future states, incur substantial computational costs and often fail to meet real-time demands, especially in navigation tasks requiring rapid responses.

To overcome these limitations, we propose a lightweight latent space-based navigation world model that reduces computational overhead and improves navigation accuracy. By mapping visual observations and tasks into latent space, our model significantly lowers search complexity and enhances decision-making efficiency in complex environments.

III. OUR APPROACH

We propose LS-NWM, a lightweight world model for image-goal navigation, as shown in Fig. 2. Given a sequence of visual observations $\mathcal{O} = \{o_1, o_2, \dots, o_n\}$ and corresponding navigation actions $\mathcal{A} = \{a_1, a_2, \dots, a_n\}$, where each action $a_t = (x_t, y_t, \theta_t)$ comprises forward translation

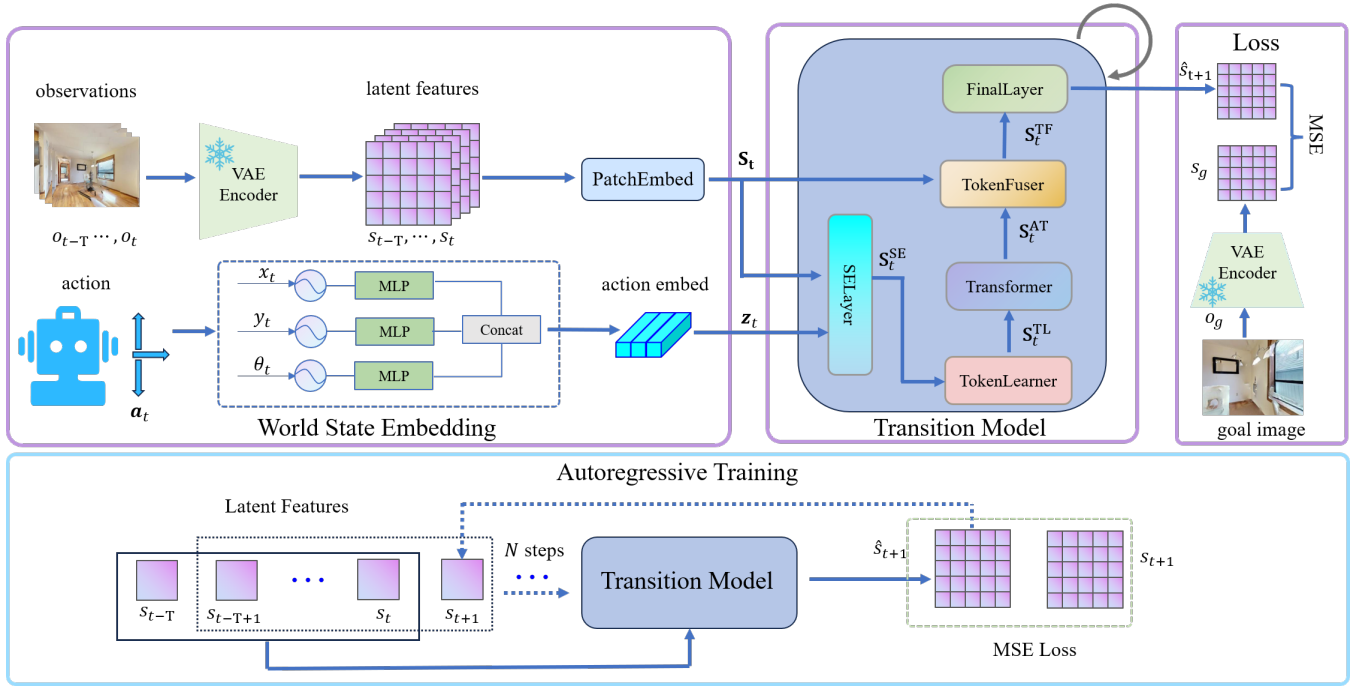


Fig. 2: The overall framework. Our world model comprises two core modules: a World State Embedding that encodes images and robot actions into latent state representations, and a Transition Model that predicts future latent states based on the embedded world state. We employ an autoregressive training strategy in which the model’s predictions are recursively fed back as input, enabling it to capture long-term spatiotemporal structures and environmental dynamics.

x_t , lateral translation y_t , and rotation angle θ_t , our model learns directly from such video-like datasets to capture the mapping from historical observations and actions to future observations. We argue that pixel-level prediction is not essential for navigation tasks. Therefore, the objective of our world model shifts toward the prediction of future implicit states. This is formalized as a state-transition model defined by:

$$s_{t+1} = p(s_{\leq t}, z_{\leq t}), \quad (1)$$

where $s_t = \text{enc}_o(o_t)$ represents the implicit state derived from the observation o_t via the observation encoder enc_o and $z_t = \text{enc}_a(a_t)$ is the implicit state derived from the action a_t via the action encoder enc_a , as detailed in Sec. III-A. $s_{\leq t} = (s_1, s_2, \dots, s_t)$ and $z_{\leq t} = (z_1, z_2, \dots, z_t)$ denote the sequences of encoded observations and actions. Further details regarding the state-transition model are provided in Sec. III-B, and the training strategy is elaborated in Sec. III-C. Finally, by incorporating Cross-Entropy Method (CEM), the world model is embedded into an end-to-end robotic navigation framework, as detailed in Sec. III-D.

A. World State Embedding

In this module, the world state is mapped into a latent space to enable effective representation and integration of environmental states within the world model. The world state comprises two components: visual observations and actions. For visual observation encoding, instead of training from scratch, we utilize a pre-trained Variational Autoencoder (VAE) [29] that incorporates large-scale data priors to ensure

consistent environmental representations and accelerate convergence. It is worth noting that our approach is compatible with arbitrary front-end feature encoders, though the VAE yielded the best performance in our experiments as detailed in Sec. IV-D.

For action encoding, we use periodic embeddings [9] to expand each action component through sine and cosine, enabling the model to be sensitive to periodic and spatial information. The action embedding layer is encoded with separate branches independently and then concatenated along the feature dimension to form a unified action vector, formulated as:

$$z_t = \text{Concat}\left(\mathbf{M}_x(\varepsilon(x_t)), \mathbf{M}_y(\varepsilon(y_t)), \mathbf{M}_\theta(\varepsilon(\theta_t))\right), \quad (2)$$

$$\varepsilon(x_t) = [\cos(x_t \cdot \omega_f), \sin(x_t \cdot \omega_f)]_{f=1}^F, \quad (3)$$

$$\omega_f = P_{\max}^{\frac{2f}{F}}, \quad f = 0, \dots, F-1, \quad (4)$$

where P_{\max} denotes the maximum period, F is the number of frequency bases, and \mathbf{M}_x , \mathbf{M}_y , and \mathbf{M}_θ correspond to MLPs applied to the respective periodic embedding branch.

B. Transition Model

Having obtained the latent representation of the current world state, we further integrate navigation context with observational features to facilitate action-conditioned prediction in the transition model.

World state fusion. As an initial step, we utilize a Squeeze-and-Excitation (SE) module [30] to adaptively recalibrate the joint representation of visual and action features, denoted

as $\mathbf{S}_t^{\text{SE}} \in \mathbb{R}^{T \times M \times D}$, where T denotes the history length, M denote the number of spatial tokens per observation, D denote the feature embedding dimension. SE module allows the model to dynamically highlight environmental aspects most relevant to the agent’s behavior, derived as:

$$\mathbf{S}_t^{\text{SE}} = \mathbf{S}_t \odot \sigma(\text{MLP}(\mathbf{z}_t)), \quad (5)$$

where \odot denotes element-wise multiplication, $\sigma(\cdot)$ denotes the sigmoid activation, and $\mathbf{S}_t = (s_{t-T+1}, \dots, s_t)$ are the past T visual observations encoded via a pretrained VAE.

To further enhance the network’s attention toward tokens that contribute more substantially to navigation decisions, we incorporate a TokenLearner module [31] to select a compact set of representative tokens. Specifically, \mathbf{S}_t^{SE} is first mapped to a set of intermediate weights \mathbf{X} through an MLP:

$$\mathbf{X} = \text{MLP}(\mathbf{S}_t^{\text{SE}}). \quad (6)$$

These weights are normalized across spatial dimensions using a softmax function. The resulting attention weights are then used to generate a compact set of latent scene representations $\mathbf{S}_t^{\text{TL}} \in \mathbb{R}^{T \times K \times D}$ that emphasize navigation-critical information, derived as follows:

$$\boldsymbol{\alpha} = \text{softmax}(\mathbf{X}), \quad (7)$$

$$\mathbf{S}_t^{\text{TL}} = \left\{ \sum_{i=1}^M \boldsymbol{\alpha}_{k,i} \cdot \mathbf{S}_t^{\text{SE}} \mid k = 1, \dots, K \right\}, \quad (8)$$

where K is the number of output tokens, i index input tokens (M in total), and k indexes the selected output tokens (K in total). These tokens retain the core information of the input while significantly reducing the computational cost for subsequent processing.

Historical embedding. Historical tokens play a crucial role in a robot’s understanding of its environment. To model the long-term dependencies between tokens, we further utilize a multi-layer attention mechanism to enhance its representational capacity. Specifically, we apply self-attention across all tokens from all historical frames to obtain the aggregated representation $\mathbf{S}_t^{\text{AT}} \in \mathbb{R}^{A \times D}$, formulated as follows:

$$\mathbf{S}_t^{\text{AT}} = \text{SelfAttention}(\mathbf{S}_t^{\text{TL}}), \quad (9)$$

Inspired by SSR [32], we also employ the TokenFuser [31] to integrate historical information. The core idea of TokenFuser is to abstract historical features through a dynamic weighting mechanism and propagate this information via a message-passing formulation to enable feature fusion across frames, formulated as:

$$\mathbf{S}_t^{\text{TF}} = \sigma(\text{MLP}(\mathbf{S}_t)) \cdot (\mathbf{W} \cdot \mathbf{S}_t^{\text{AT}} + \mathbf{d})^\top, \quad (10)$$

where \mathbf{W} and \mathbf{d} are the parameters of the linear projection, $\sigma(\cdot)$ denotes the sigmoid activation, and $\mathbf{S}_t^{\text{TF}} \in \mathbb{R}^{T \times M \times D}$ is the fused feature map aligned with the spatial structure.

Future state prediction. At the final stage of the transition model, we employ a set of MLPs to map the fused features \mathbf{S}_t^{TF} into the predicted future state \hat{s}_{t+1} , formulated as follows:

$$\hat{s}_{t+1} = \text{MLP}(\text{Conv}(\mathbf{S}_t^{\text{TF}})), \quad (11)$$

where $\text{Conv}(\cdot)$ performs convolutional aggregation over the feature sequence.

C. Training Policy

Our world model is trained to predict future implicit states based on the current world state. In contrast to pixel-level supervision of future states, we directly supervise the predicted sparse implicit representations during training. Since navigation is inherently a long-horizon planning problem, accurate long-horizon predictions are crucial. To enhance long-term predictive consistency, we employ multi-step supervision, guiding the model to generate coherent future states over extended periods.

Specifically, we iteratively uses the predicted output along with ground-truth actions as input for subsequent predictions. This process continues for N steps, with supervision applied at each step. Although this approach increases training difficulty, our model’s lightweight design—combined with avoiding photorealistic reconstruction—keeps computational costs within practical limits. We optimize the model using a mean squared error (MSE) loss function to minimize the discrepancy between predicted and ground-truth latent features, formulated as:

$$\hat{s}_{t+1} = p_\theta(\mathbf{S}_t, \mathbf{z}_t), \quad (12)$$

$$\hat{s}_{t+k+1} = p_\theta(\hat{\mathbf{S}}_{t+k}, \mathbf{z}_{t+k}), \quad k \geq 1, \quad (13)$$

$$\mathcal{L} = \frac{1}{N} \sum_{k=1}^N \|\hat{s}_{t+k} - s_{t+k}\|^2, \quad (14)$$

where $\hat{\mathbf{S}}_{t+k} = (s_{t+k-T+1}, \dots, s_{t-1}, s_t, \hat{s}_{t+1}, \dots, \hat{s}_{t+k})$, p_θ denotes our overall transition model, and θ represents the learnable model parameters. Based on this autoregressive rollout, the training objective is defined as the mean squared error (MSE) between the predicted sequence and the ground-truth future states. This autoregressive training mechanism enables the model to capture temporal dependencies across multiple steps, thereby improving the accuracy of long-horizon predictions.

D. Image-goal navigation with LS-NWM

In the image-goal navigation task, given a target image, the robot needs to reach the position corresponding to the target image based on its current observation. Using our latent space navigation world model, we predict a sequence of future states from the initial state and potential action sequences. Specifically, given the robot’s current state s_0 and action sequence $(\mathbf{a}_0, \dots, \mathbf{a}_{t-1})$, our model autoregressively outputs a sequence of future states $\hat{s}_1, \dots, \hat{s}_t$. Our goal is to find the optimal action sequence $(\mathbf{a}_0, \dots, \mathbf{a}_{t-1})$ that maximizes the likelihood of reaching the VAE encoding of the target image state s_g . To achieve this, we define an energy function to compute the energy values of states:

$$E(\hat{s}_t, s_g) = -L(\hat{s}_t, s_g), \quad (15)$$

where $L(\hat{s}_t, s_g)$ represents the L2 loss between the final state and the target state. This transforms the problem into finding the action sequence that minimizes the energy function.

Consequently, the entire problem is framed as a Model Predictive Control (MPC) problem [9].

IV. EXPERIMENTAL EVALUATION

We conduct experiments to evaluate the effectiveness of the proposed method. First, we tested the performance of our approach in trajectory prediction and demonstrated its state-of-the-art (SOTA) performance in long-term trajectory prediction, as detailed in Sec. IV-A. Subsequently, we evaluated the proposed navigation world model on image-goal navigation tasks, demonstrating its advantages in navigation accuracy and generalization, as elaborated in Sec. IV-B. We further validated the significant efficiency advantages of our method in terms of runtime compared to existing world model approaches, as presented in Sec. IV-C. Finally, ablation studies analyzing the contributions of each component are provided in Sec. IV-D.

We set the context window size to $T = 4$ and the number of prediction steps for future states to $N = 4$, using VAE-encoded features as supervisory signals with a batch size of 256. Training was conducted on 2 A100 GPUs. Trajectories generated in the experiments had a length of 8.

A. Trajectory Prediction Performance

To comprehensively evaluate the effectiveness of the proposed world model, we first conduct experiments on trajectory prediction within the image-goal visual navigation task. We benchmark our method against several state-of-the-art end-to-end navigation models, including: the end-to-end trajectory generation approach GNM [4], NoMaD [6], as well as world model-based navigation approaches such as NWM [9]. All baseline methods use the default settings, with the number of diffusion steps for NWM is set to 250.

Datasets. We follow the experimental protocol established by NoMaD and utilize four publicly available datasets to train and evaluate our world model. These datasets comprise first-person RGB images captured by robotic platforms, accompanied by pose information that enables inference of the robot’s actions. Specifically: the SCAND dataset [33] includes social navigation data collected using both wheeled and legged robots. The RECON dataset [34] contains trajectories from outdoor robot navigation scenarios. The Tartan dataset [35] focuses on field robot navigation in diverse unstructured environments. The HuRoN dataset [36] features robotic social interaction navigation tasks. Multi-datasets ensure broad coverage of navigation contexts and enhances the generalization capability of our model.

Evaluation Metrics: We use the following two metrics for evaluation: i) Absolute Trajectory Error (ATE): Measures the global consistency of the trajectory by computing the absolute difference between predicted and ground-truth robot positions. ii) Relative Pose Error (RPE): Evaluates local accuracy by measuring the relative pose discrepancy between consecutive predicted and true robot positions.

Results: As shown in Tab. I, our approach demonstrates remarkable performance in both ATE and RTE when predicting trajectories of up to 2 seconds across most datasets. Our

model’s size is comparable to end-to-end trajectory generation methods and significantly smaller than the world model-based approach NWM, yet it achieves comparable or even superior trajectory prediction accuracy. These results fully demonstrate its efficiency and competitiveness in trajectory prediction for image-goal visual navigation tasks.

B. Visual Navigation Performance

To further validate the navigation performance and generalization capability of the proposed model under conditions closely resembling real-world physical interactions, we randomly selected 10 image-goal navigation episodes from the Gibson dataset. Ground-truth (GT) trajectories were generated using the shortest-path planner provided in Habitat. At each step, our method, along with NWM, predicts the next action based on the current observation and the target image until the agent reaches within 2 m of the goal. In this experiment, we conduct comparisons exclusively with NWM, as GNM and NoMaD require pre-built topological maps of the environment and is not capable of performing end-to-end image-goal navigation like NWM and LS-NWM.

Datasets. We constructed a closed-loop testing environment using Habitat—a widely adopted robotic navigation simulation platform—and employed the Gibson dataset to provide realistic simulation scenes for experimental evaluation. The Gibson scene library comprises various high-fidelity indoor and outdoor scenes (such as family residences, office spaces, and community streets). Its scene layout complexity, texture details, and lighting diversity are highly consistent with the real world, enabling it to effectively simulate challenges that robots may encounter in practical navigation, such as visual occlusion and scene semantic variation. This provides a reasonable testing benchmark for evaluating the robustness of the model.

Evaluation Metrics. We evaluate navigation performance using success rate (SR) and Success rate weighted by Path Length (SPL).

Results. As shown in Table II, our method achieves an SR of 55%, improving state-of-the-art baseline by 35%. Furthermore, our approach also attains a better SPL, outperforming NWM by 11%. These results demonstrate that our autonomous navigation framework is both more reliable and more efficient.

We visualize the navigation path of our method in comparison to NWM within the Habitat simulator. As shown in Fig. 4, our trajectories (red) are more closer to the ground-truth shortest path (blue) than those generated by NWM (green), which show clear deviations across multiple segments. Note that the original implementation of NWM incurs a computational cost of approximately 200 seconds for inference. To ensure a fair comparison and reduce computational overhead, we decreased the number of diffusion steps in NWM from 250 to 6, following its recommended practice for efficiency. Nevertheless, LS-NWM maintains a substantial efficiency advantage over NWM, as quantitatively demonstrated in Sec. IV-C. The slight lateral drift observed in our trajectories stems from the robot’s tendency to exhibit

TABLE I: Trajectory Prediction Performance. ATE and RPE results across all in-domain datasets for trajectories predicted up to 2 seconds.

model	params	RECON		HuRoN		Tartan		SCAND	
		ATE	RTE	ATE	RTE	ATE	RTE	ATE	RTE
GNM	8M	1.87	0.73	3.71	1.00	6.65	1.62	2.12	0.61
NoMaD	19M	1.95	0.53	3.73	0.96	6.32	1.31	2.24	0.49
NWM	1B	1.13	0.35	4.12	0.96	5.63	1.18	1.28	0.33
Ours	30M	1.51	0.43	4.54	0.94	5.35	1.13	1.28	0.32

The best results are highlighted in bold.

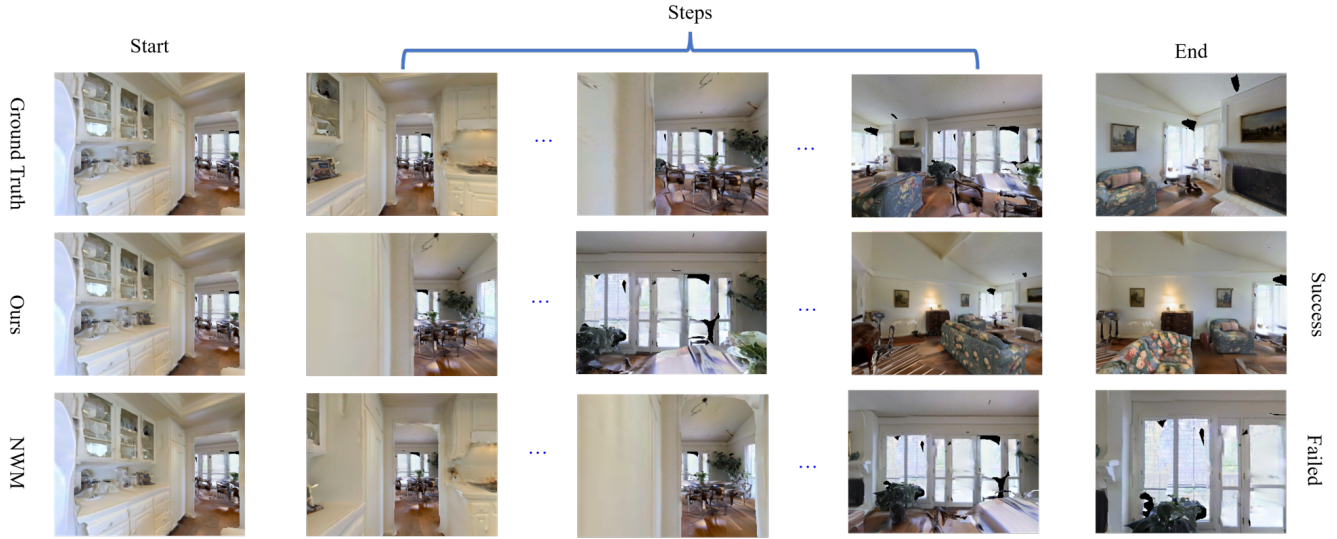


Fig. 3: Visualization of the navigation process in the image-goal navigation task.

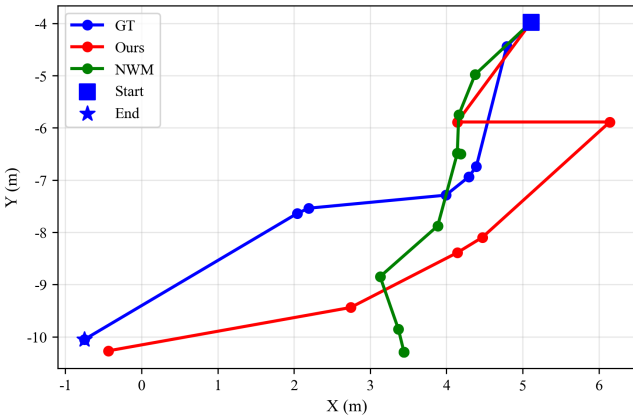


Fig. 4: Trajectory comparison between our method and NWM in the image-goal navigation task.

minor sideways deviations while tracking target points. These small errors can occasionally accumulate over time, resulting in larger displacements.

To further analyze navigation behavior, Fig. 3 offers a step-by-step visualization of the decision sequence. Each row corresponds to the agent’s visual observations at consecutive action steps. The comparison confirms that our method produces trajectories that adhere more faithfully to the intended path, whereas NWM often diverges, taking detours or misaligning with the target—ultimately resulting

TABLE II: Navigation Performance.

Method	SR	SPL
NWM	20.0%	20.0%
Ours	55.0%	30.9%

The best results are highlighted in bold.

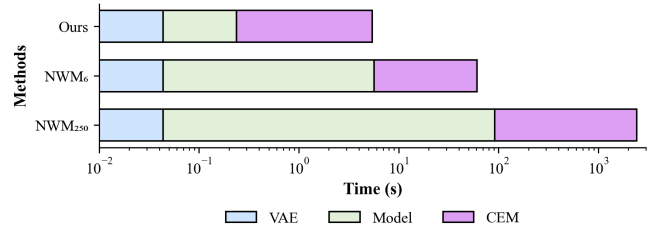


Fig. 5: Runtime Analysis.

in navigation failures.

C. Runtime Analysis

To demonstrate the efficiency of our model, we compare the runtime of our method and NWM for navigation planning. The Cross-Entropy Method (CEM) sampling is uniformly configured with 120 samples and optimized over 3 iterations. We compare the runtime of our method with NWM₂₅₀ (using default settings and 250 diffusion steps) and NWM₆ (using the recommended practical configuration with

TABLE III: Ablation Studies of Individual Modules. Default structure are marked in gray and the best results are highlighted in bold.

(a) TokenLearner & TokenFuser			(b) Latent or explicit		
model	SCAND		model	SCAND	
	ATE	RTE		ATE	RTE
With	1.28	0.32	Latent Space	1.28	0.32
Without	1.32	0.34	Explicit	1.31	0.33

(c) Number of predict frames			(d) Visual encoder		
num	SCAND		encoder	SCAND	
	ATE	RTE		ATE	RTE
1	1.38	0.35	VAE	1.28	0.32
4	1.28	0.32	DINOv2	1.65	0.39
			R3M	2.22	0.49

6 diffusion steps). As shown in Fig. 5, our approach achieves substantial efficiency advantage. Specifically, planning a single path takes 5.2 s with our method, while NWM₂₅₀ requires 2329.2 s and NWM₆ requires 55 s. This corresponds to a speedup of approximately 447× compared to NWM₂₅₀ and 10× compared to NWM₆. These results underscore that our framework drastically reduces computational requirements, thereby enabling real-time performance and enhancing practical deployability.

D. Ablation Study

To evaluate the effectiveness of our model, we conducted experiments on several architectural variants using the trajectory prediction task. All evaluations were performed consistently on the SCAND dataset.

TokenLearner & TokenFuser. To evaluate the contribution of the TokenLearner and TokenFuser modules, we performed ablation studies by removing each module individually and feeding fused features directly into the Transformer for prediction. We then compared the navigation performance of each ablated model against the full proposed framework.

As shown in Tab. IIIa, the inclusion of both modules reduces ATE by approximately 3.0% and RTE by about 5.9%. This improvement in trajectory accuracy can be attributed to the synergistic effect of TokenLearner and TokenFuser. Their combined operation enables more precise modeling of the "observation–action–future state" mapping relationship, ultimately enhancing the trajectory precision in image-goal navigation tasks.

Latent Space or Explicit Image. We compared the performance of our model trained in latent space against a version trained using explicit image decoding. Navigation success was evaluated based on the LPIPS similarity [37] between real observations and target images, and trajectory prediction performance was assessed using standard geometric error metrics.

As shown in Table IIIb, the latent space model outperformed the explicit image-based model across both evaluation criteria. This improvement can be attributed to the

latent representation's ability to retain semantically salient navigation features more efficiently while filtering out redundant visual information, thereby achieving higher navigation accuracy.

Number of predict frames. Our network employs, by default, an autoregressive multi-step training strategy with $N = 4$ steps. To evaluate the effectiveness of this design, we compare the trajectory prediction performance under two distinct training configurations: a single-step setup ($N = 1$) and the multi-step setup ($N = 4$).

As shown in Tab. IIIc, the model achieves best performance under the multi-step configuration ($N = 4$). This improvement can be attributed to the inherent nature of trajectory prediction as a long-horizon planning task, which requires the network to capture temporal dependencies over extended sequences. By explicitly supervising multi-step predictions during training, the model learns to maintain consistency and accuracy across longer time spans, resulting in superior overall performance.

Visual encoder. We conduct an ablation study on the visual encoder by comparing the trajectory prediction performance of our model using different pre-trained visual encoders, namely DINOv2 [38] and R3M [39].

As shown in Tab. IIId, the VAE-based encoder proves to be the most suitable visual feature extraction module for our model, outperforming the other two encoders. This can be attributed to the VAE's ability to learn low-dimensional, compact representations that capture the core structure of the data. For navigation and positioning tasks, discriminative features that distinguish spatial locations and represent scene geometry and texture are essential. The VAE preserves spatially relevant features such as object layout and wall texture by imposing reconstruction constraints on the visual input. Furthermore, the low-dimensional nature of its features reduces redundant interference and computational noise for subsequent positioning modules, resulting in optimal performance in both ATE and RTE metrics.

V. CONCLUSION

In this paper, we present LS-NWM, a lightweight world model for image-goal navigation. Instead of relying on computationally expensive pixel-level prediction, our approach predicts compact latent future states and performs navigation planning directly in this latent representation, significantly reducing model size and computational requirements. We employ an autoregressive training strategy to enhance the model's accuracy in long-horizon environmental prediction. Our model outperforms state-of-the-art world model-based methods as well as end-to-end trajectory generation approaches across multiple datasets while maintaining lightweight efficiency. Future work will focus on validation through real-world robot experiments and extension to dynamic environments.

REFERENCES

[1] J. Huang, B. Zhou, Z. Fan, Y. Zhu, Y. Jie, L. Li, and H. Cheng, "Fael: Fast autonomous exploration for large-scale environments with

a mobile robot,” *IEEE Robotics and Automation Letters*, vol. 8, no. 3, pp. 1667–1674, 2023.

[2] F. Yang, C. Cao, H. Zhu, J. Oh, and J. Zhang, “Far planner: Fast, attemptable route planner using dynamic visibility update,” in *2022 ieee/rsj international conference on intelligent robots and systems (iros)*. IEEE, 2022, pp. 9–16.

[3] C. Cao, H. Zhu, H. Choset, and J. Zhang, “Exploring large and complex environments fast and efficiently,” in *2021 IEEE international conference on robotics and automation (ICRA)*. IEEE, 2021, pp. 7781–7787.

[4] D. Shah, A. Sridhar, A. Bhorkar, N. Hirose, and S. Levine, “GNM: A General Navigation Model to Drive Any Robot,” in *International Conference on Robotics and Automation (ICRA)*, 2023. [Online]. Available: <https://arxiv.org/abs/2210.03370>

[5] D. Shah, A. Sridhar, N. Dashora, K. Stachowicz, K. Black, N. Hirose, and S. Levine, “ViNT: A foundation model for visual navigation,” in *7th Annual Conference on Robot Learning*, 2023. [Online]. Available: <https://arxiv.org/abs/2306.14846>

[6] A. Sridhar, D. Shah, C. Glossop, and S. Levine, “Nomad: Goal masked diffusion policies for navigation and exploration,” in *2024 IEEE International Conference on Robotics and Automation (ICRA)*. IEEE, 2024, pp. 63–70.

[7] S. Xinyu, C. Peihao, F. Jugang, H. L. Thomas, C. Jian, and T. Mingkui, “Fgprompt: Fine-grained goal prompting for image-goal navigation,” in *37th Conference on Neural Information Processing Systems (NeurIPS 2023)*, 2023.

[8] K.-H. Zeng, Z. Zhang, K. Ehsani, R. Hendrix, J. Salvador, A. Herrasti, R. Girshick, A. Kembhavi, and L. Weihs, “Poliformer: Scaling on-policy rl with transformers results in masterful navigators,” *CoRL*, 2024.

[9] A. Bar, G. Zhou, D. Tran, T. Darrell, and Y. LeCun, “Navigation world models,” in *Proceedings of the Computer Vision and Pattern Recognition Conference*, 2025, pp. 15 791–15 801.

[10] J. Ding, Y. Zhang, Y. Shang, Y. Zhang, Z. Zong, J. Feng, Y. Yuan, H. Su, N. Li, N. Sukiennik, et al., “Understanding world or predicting future? a comprehensive survey of world models,” *ACM Computing Surveys*, 2024.

[11] H. Wang, W. Liang, L. Van Gool, and W. Wang, “Dreamwalker: Mental planning for continuous vision-language navigation,” in *Proceedings of the IEEE/CVF international conference on computer vision*, 2023, pp. 10 873–10 883.

[12] J. Y. Koh, H. Lee, Y. Yang, J. Baldridge, and P. Anderson, “Path-dreamer: A world model for indoor navigation,” in *Proceedings of the IEEE/CVF International Conference on Computer Vision*, 2021, pp. 14 738–14 748.

[13] D. S. Chaplot, R. Salakhutdinov, A. Gupta, and S. Gupta, “Neural topological slam for visual navigation,” in *Proceedings of the IEEE/CVF conference on computer vision and pattern recognition*, 2020, pp. 12 875–12 884.

[14] Y. Cui, S. Ye, X. Xu, H. Sha, C. Wang, L. Lin, Z. Liu, R. Xiong, and Y. Wang, “Learning hierarchical graph-based policy for goal-reaching in unknown environments,” *IEEE Robotics and Automation Letters*, vol. 9, no. 6, pp. 5655–5662, 2024.

[15] L. Mezghan, S. Sukhbaatar, T. Lavril, O. Maksymets, D. Batra, P. Bojanowski, and K. Alahari, “Memory-augmented reinforcement learning for image-goal navigation,” in *2022 IEEE/RSJ International Conference on Intelligent Robots and Systems (IROS)*. IEEE, 2022, pp. 3316–3323.

[16] W. Cai, J. Peng, Y. Yang, Y. Zhang, M. Wei, H. Wang, Y. Chen, T. Wang, and J. Pang, “Navdp: Learning sim-to-real navigation diffusion policy with privileged information guidance,” *arXiv preprint arXiv:2505.08712*, 2025.

[17] K. Zhou, K. Zheng, C. Pryor, Y. Shen, H. Jin, L. Getoor, and X. E. Wang, “Esc: Exploration with soft commonsense constraints for zero-shot object navigation,” in *International Conference on Machine Learning*. PMLR, 2023, pp. 42 829–42 842.

[18] S. Y. Gadre, M. Wortsman, G. Ilharco, L. Schmidt, and S. Song, “Cows on pasture: Baselines and benchmarks for language-driven zero-shot object navigation,” in *Proceedings of the IEEE/CVF Conference on Computer Vision and Pattern Recognition*, 2023, pp. 23 171–23 181.

[19] B. Yu, H. Kasaei, and M. Cao, “L3mvn: Leveraging large language models for visual target navigation,” in *2023 IEEE/RSJ International Conference on Intelligent Robots and Systems (IROS)*. IEEE, 2023, pp. 3554–3560.

[20] W. Cai, S. Huang, G. Cheng, Y. Long, P. Gao, C. Sun, and H. Dong, “Bridging zero-shot object navigation and foundation models through pixel-guided navigation skill,” in *2024 IEEE International Conference on Robotics and Automation (ICRA)*. IEEE, 2024, pp. 5228–5234.

[21] Y. Hu, L. Wang, X. Liu, L.-H. Chen, Y. Guo, Y. Shi, C. Liu, A. Rao, Z. Wang, and H. Xiong, “Simulating the real world: A unified survey of multimodal generative models,” *arXiv preprint arXiv:2503.04641*, 2025.

[22] D. Hafner, J. Pasukonis, J. Ba, and T. Lillicrap, “Mastering diverse control tasks through world models,” *Nature*, pp. 1–7, 2025.

[23] D. Hafner, T. Lillicrap, M. Norouzi, and J. Ba, “Mastering atari with discrete world models,” *arXiv preprint arXiv:2010.02193*, 2020.

[24] D. Huang, J. Wang, Y. Li, C. Xia, T. Zhang, and K. Zhang, “Pig-dreamer: Privileged information guided world models for safe partially observable reinforcement learning,” *arXiv preprint arXiv:2508.02159*, 2025.

[25] D. Nie, X. Guo, Y. Duan, R. Zhang, and L. Chen, “Wmnav: Integrating vision-language models into world models for object goal navigation,” *arXiv preprint arXiv:2503.02247*, 2025.

[26] W. Liu, H. Zhao, C. Li, J. Biswas, B. Okal, P. Goyal, Y. Chang, and S. Pouya, “X-mobility: End-to-end generalizable navigation via world modeling,” *arXiv preprint arXiv:2410.17491*, 2024.

[27] Y. Qin, A. Sun, Y. Hong, B. Wang, and R. Zhang, “Navigatediff: Visual predictors are zero-shot navigation assistants,” *arXiv preprint arXiv:2502.13894*, 2025.

[28] H. Ren, Y. Zeng, Z. Bi, Z. Wan, J. Huang, and H. Cheng, “Prior does matter: Visual navigation via denoising diffusion bridge models,” in *Proceedings of the Computer Vision and Pattern Recognition Conference*, 2025, pp. 12 100–12 110.

[29] A. Blattmann, T. Dockhorn, S. Kulal, D. Mendelevitch, M. Kilian, D. Lorenz, Y. Levi, Z. English, V. Voleti, A. Letts, et al., “Stable video diffusion: Scaling latent video diffusion models to large datasets,” *arXiv preprint arXiv:2311.15127*, 2023.

[30] J. Hu, L. Shen, and G. Sun, “Squeeze-and-excitation networks,” in *Proceedings of the IEEE conference on computer vision and pattern recognition*, 2018, pp. 7132–7141.

[31] M. Ryoo, A. Piergiovanni, A. Arnab, M. Dehghani, and A. Angelova, “Tokenlearner: Adaptive space-time tokenization for videos,” *Advances in neural information processing systems*, vol. 34, pp. 12 786–12 797, 2021.

[32] P. Li and D. Cui, “Navigation-guided sparse scene representation for end-to-end autonomous driving,” in *International Conference on Learning Representations (ICLR)*, 2025.

[33] H. Karnan, A. Nair, X. Xiao, G. Warnell, S. Pirk, A. Toshev, J. Hart, J. Biswas, and P. Stone, “Socially compliant navigation dataset (scand): A large-scale dataset of demonstrations for social navigation,” *IEEE Robotics and Automation Letters*, 2022.

[34] D. Shah, B. Eysenbach, G. Kahn, N. Rhinehart, and S. Levine, “Rapid exploration for open-world navigation with latent goal models,” *arXiv preprint arXiv:2104.05859*, 2021.

[35] S. Triest, M. Sivaprakasam, S. J. Wang, W. Wang, A. M. Johnson, and S. Scherer, “Tartandrive: A large-scale dataset for learning off-road dynamics models,” in *2022 International Conference on Robotics and Automation (ICRA)*. IEEE, 2022, pp. 2546–2552.

[36] N. Hirose, D. Shah, A. Sridhar, and S. Levine, “Sacosn: Scalable autonomous control for social navigation,” *IEEE Robotics and Automation Letters*, vol. 9, no. 1, pp. 49–56, 2023.

[37] R. Zhang, P. Isola, A. A. Efros, E. Shechtman, and O. Wang, “The unreasonable effectiveness of deep features as a perceptual metric,” in *Proceedings of the IEEE conference on computer vision and pattern recognition*, 2018, pp. 586–595.

[38] M. Oquab, T. Darce, T. Moutakanni, H. V. Vo, M. Szafraniec, V. Khalidov, P. Fernandez, D. Haziza, F. Massa, A. El-Nouby, R. Howes, P.-Y. Huang, H. Xu, V. Sharma, S.-W. Li, W. Galuba, M. Rabbat, M. Assran, N. Ballas, G. Synnaeve, I. Misra, H. Jegou, J. Mairal, P. Labatut, A. Joulin, and P. Bojanowski, “Dinov2: Learning robust visual features without supervision,” 2023.

[39] S. Nair, A. Rajeswaran, V. Kumar, C. Finn, and A. Gupta, “R3m: A universal visual representation for robot manipulation,” *arXiv preprint arXiv:2203.12601*, 2022.